ELSEVIER

Biophysical Chemistry 53 (1995) 267–281

Biophysical Chemistry

Superstructural features of the upstream regulatory regions of two pea *rbcS* genes and nucleosomes positioning: theoretical prediction and experimental evaluation

S. Cacchione [a], M.A. Cerone [a], P. De Santis [b], M. Savino [a,*]

[a] *Dipartimento di Genetica e Biologia Molecolare, Università di Roma I, La Sapienza, P. le Aldo Moro, 5 00185 Roma, Italy*

[b] *Dipartimento di Chimica-Università di Roma I, La Sapienza, Roma, Italy*

Received 13 June 1994; accepted in revised form 2 August 1994

Abstract

Nucleosome positioning on two 384 bp DNA fragments, obtained from the upstream regulatory region of two pea *rbcS* genes, relevant in photoregulated transcription, was predicted using our theoretical method, based on the evaluation of the sequence dependent DNA bending energy. The theoretical prediction was checked by experimental evaluation of nucleosome positions after in vitro reconstitution, by mapping Exonuclease III-resistant borders and by digesting monomeric sequences with various restriction enzymes. Both approaches satisfactorily confirmed the theoretical predictions, showing that the nucleotide sequence intrinsic bendability has a dominant role in nucleosome positioning.

Keywords: DNA superstructures; Nucleosome positioning; *rbcS* genes; Theoretical prediction

1. Introduction

It is now generally accepted that DNA superstructural features, depending on the fluctuations of the base sequence, in phase with the periodicity of the B double helix, are relevant to its physico-chemical properties as well as its biological behaviour.

Although the physicochemical origin of DNA curvature is still a matter of debate, sound evidence has been accumulated of a major contribution of the nearest-neighbor differential interactions within the dinucleotide steps [1–5].

We have previously shown that DNA curvature can be predicted, integrating the slight local deviations in terms of roll and tilt angles, obtained on the basis of energy conformational calculations for the 16 dinucleotide steps [2,3].

This method was successfully applied to predict the curvature of numerous synthetic as well as natural DNAs and is found to be in surprisingly good agreement with experimental measurements, based on gel electrophoretic retardations and cyclization kinetics [4,6].

Besides the prediction of intrinsic DNA curvature, the method appears successful in predicting DNA induced superstructures due to nucleosome formation, since the correlation between the theoretical analysis and experimental evaluation in a number of systems of biological interest, reported in the literature, is very satisfactory [7,8].

The results obtained, encouraged us to take advantage of the theoretical method, in studying nucleosomes

* Corresponding author.

SSDI 0301-4622(94)00105-7

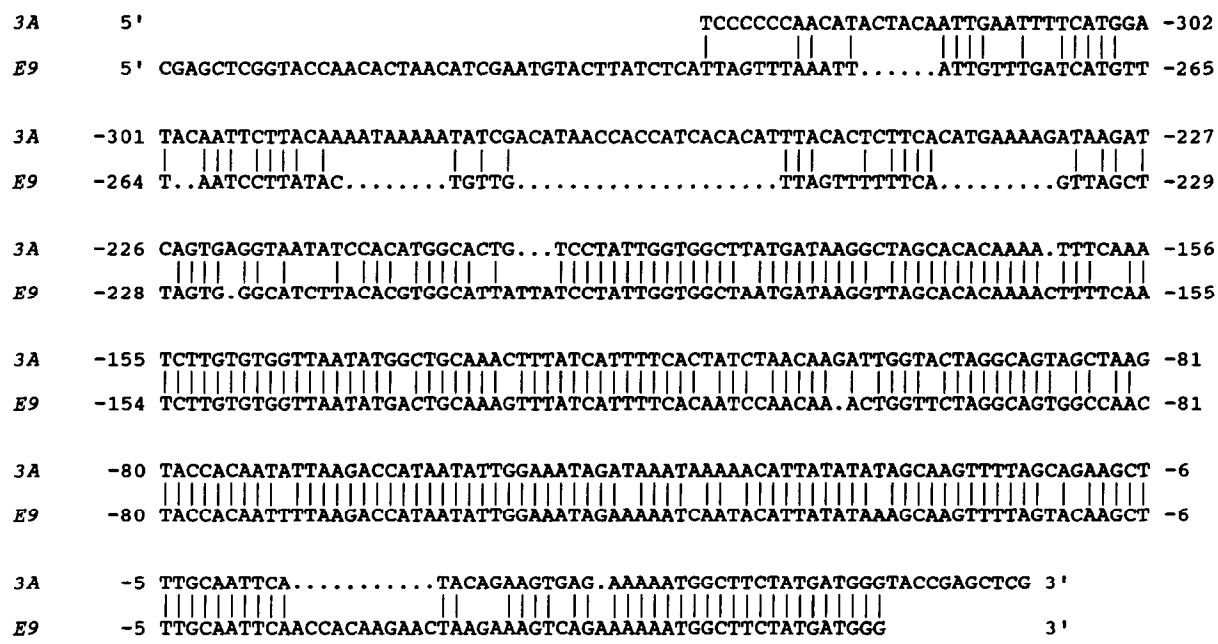

Fig. 1. Sequences of the DNA fragments 384-3A and 384-E9. Sequences are aligned to show similarities. Sequences homology was estimated as 83% on the whole region under examination and 90% in the region between −200 and +50 with respect to the transcription origin. Alignment and homology estimation was done using the best fit program [27].

organization on DNA regulatory sequences, since nucleosome positioning on these regions seems to play an active role in the regulation of basic biological processes such as DNA replication and transcription [9–11].

In this paper, we have analyzed both theoretically and experimentally, by Exonuclease III (Exo III) and restriction enzymes selective DNA cleavage, nucleosome positioning on two 384 bp fragments from the regulatory regions of two pea genes, *rbcS-3A* and *rbcS-E9*, that encode the small subunit of ribulose-1,5-bisphosphate carboxylase (a key enzyme in photosynthesis). The largely different transcription efficiency of these two genes (*rbcS-3A*, 40% of the total transcript; *rbcS-E9*, less than 7% [12]) has been connected, on the basis of genetic and biochemical analysis, to the upstream regulative region from about −400 to the start site of transcription [13]. The region between −164 and −114, containing three short sequences (Box I, Box II, and Box III) conserved in all *rbcS* genes [14], has been named the light responsive element (LRE) because it confers light responsiveness and tissue specificity [14,15]. Box II and Box III, situated between −151 and −114, bind to the regulative protein GT1 [15].

We have previously studied the superstructural features of the two regulative regions by theoretical analysis and cyclization kinetics. In spite of the remarkable sequence homology (see Fig. 1 legend), their superstructural features are different; in fact *rbcS-3A*, the most transcribed *rbcS* gene, presents an higher curvature of the 5′ regulative region with respect to that of the *rbcS-E9* gene [6].

In this paper we show that the difference in superstructural features of the regulative regions of the two *rbcS* genes are relevant, not only in cyclization kinetics, but also in nucleosome positioning; in fact we find that nucleosome preferential locations are quite different in the two cases. We have analyzed the positioning of only one nucleosome on the two 384 bp DNA fragments (see Fig. 1), although up to two nucleosomes could be accomodated on the two DNA fragments. The choice of a nonsaturated system allows us to compare theoretical distortion energy profiles with nucleosome positioning, avoiding the effects of nucleosome–nucleosome interactions. The results obtained strongly support the main role of DNA intrinsic flexibility in nucleosome positioning and the satisfactory predictive power of our method. Furthermore, these results indicate that differences in nucleosome positioning could

be relevant to the large difference in transcription efficiency of the two genes.

2. Materials and methods

2.1. Materials

Restriction endonucleases, T4 polynucleotide kinase, and Exonuclease III were from USB; micrococcal nuclease was from Pharmacia; *Taq* DNA polymerase was from Promega; radiolabelled chemicals were from Amersham.

2.2. DNAs

The DNA fragments 384-3A and 384-E9 were obtained respectively from an *Hae*III-*Eco*RV fragment (−331/+36) from the clone pUC18-3A/E9 [12], and from an *Hin*cII/*Eco*RV fragment (−320/+47) from the clone pBR325-E9 [16]. The two DNAs were then ligated into the *Sma*I site of pUC18. Plasmids were prepared by the alkaline lysis method. Two different labelling procedures were followed: in order to obtain DNA fragments 5′ labelled on only one strand for the Exonuclease III experiments, plasmids were linearized with *Eco*RI or *Bam*HI, situated at either side of the inserts, and 5′ labelled with T4 Kinase and [γ-^{32}P]dATP; the 384 bp fragments were obtained with a second digestion with either *Eco*RI or *Bam*HI, and electroeluted after electrophoresis on agarose gel. For restriction enzyme digestion experiments, fragments were produced by 30 cycles PCR synthesis in the presence of [α-^{32}P]dATP, in order to obtain internally labelled DNAs (dATP/[α-^{32}P]dATP molar ratio, 500). The sequences of the two DNA fragments are reported in Fig. 1.

2.3. Nucleosome reconstitution

Nucleosome core particles were prepared from chicken erythrocyte chromatin digested with micrococcal nuclease and purified through 5–20% sucrose gradient ultracentrifugation [17]. Nucleosomes were reconstituted on 200 ng (10^5 cpm) radiolabelled DNA fragments according to the salt dilution protocol [18] starting from 0.85 M NaCl to 0.05 M NaCl. Reconstitution was performed at fixed nucleosome/labeled DNA ratios (10/1), with different amounts of nucleosomal DNA as competitor. The reconstitutes were analyzed for resistance to micrococcal nuclease digestion. The normal nucleosome pattern was observed (data not shown). Reconstitution was monitored by gel electrophoresis in 0.8% (w/v) agarose in 0.5×TBE buffer (45 mM Tris/45 mM boric acid/1 mM EDTA). To assess the purity of the mononucleosome preparation, reconstituted samples were separated from the remaining free DNA and nonspecific aggregates by ultracentrifugation through a 5 to 30% glycerol gradient in 50 mM Tris–HCl (pH 7.4), 1 mM EDTA, 1 mM dithiothreitol, 0.1 mM phenylmethylsulfonylfluoride, and 0.1 mg/ml bovine serum albumin, using a SW40 ultracentrifuge rotor at 35 000 revs/min for 20 h at 4°C.

2.4. Exonuclease III analysis

Reconstituted samples were made with 66 mM Tris–HCl (pH 8), 1.66 mM $MgCl_2$, and 1 mM 2-mercaptoethanol. Exonuclease III digestions were carried out at 30°C; samples were withdrawn at appropriate intervals and reactions stopped by adding an equal volume of 15 mM EDTA, 1% (w/v) sodium dodecylsulfate, and heating at 100°C for 2 min. Following extraction with phenol and precipitation with ethanol, the samples were analysed on 6% denaturing polyacrylamide gels. Gels were dried and autoradiographed; autoradiographs were analyzed with an LKB laser densitometer.

2.5. Restriction enzyme analysis

Reconstituted samples were digested for 5 min at 37°C with micrococcal nuclease (2 U/ml), in 10 mM Tris–HCl/1 mM $CaCl_2$ buffer. After proteinase K treatment and phenol extraction, the nucleosomal DNA was subjected to electrophoresis on a 6% native polyacrylamide gel and purified by electroelution. Purified monomer DNA was then digested with restriction enzymes and analyzed on 6% polyacrylamide gels.

3. Results

3.1. Theoretical prediction of nucleosome positioning

Nucleosome positioning along a DNA sequence is defined by two parameters: the translation, marking

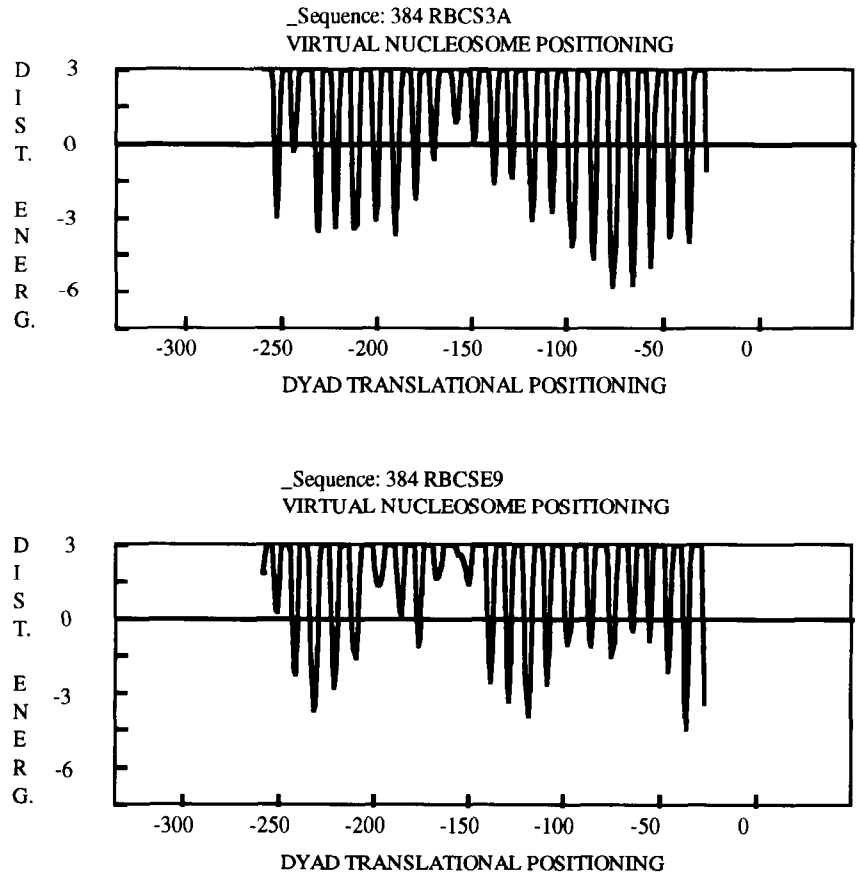

Fig. 2. The distortion energy (kcal/nucleosome) of recurrent 145 bp DNA tracts, with respect to that of an equivalent tract of a straight DNA represented by the zero line, is reported for each of the possible positions of the nucleosome dyad axis. Only the energy values less than 3 kcal/nucleosome are reported. Each minimum represents a virtual position of a nucleosome spanning a DNA tract 72 bp on both sides. The average distance between the minima is 10.3, as evaluated via Fourier transformation. (a) 384-3A and (b) 384-E9.

where the histone octamer dyad axis is placed, and the orientation of the octamer dyad axis relative to the direction of the average curvature. Many authors agree that little is known about the translation, whereas the rotational parameters appear to involve structures where the A/T rich minor grooves face in towards the protein core [19,20]. Recently, we have developed a theoretical method to obtain the virtual nucleosome positioning from the sequence by localizing the minima of the DNA bendability energy function. This was evaluated adopting our theoretical method of the sequence dependent curvature and assuming a principle of minimum deformation energy (in a simple harmonic approximation) of the intrinsic superstructure necessary to obtain the induced superstructure [8].

Therefore, recurrent 145 bp tracts along a DNA sequence were constrained to deform in agreement with an "open model" of the nucleosomal superstructure, as characterized by two 60 bp tracts of a regular superhelix of 3/4 turns with 43 Å radius and 28 Å pitch interconnected by a straight tract 25 bp long. Such a model contains a dyad axis perpendicular to the superhelical axis and was adopted on account of the superstructural features of nucleosomal DNA [19].

If $c(n)$ and $c'(n)$ are the starting intrinsic curvature function of a 145 bp DNA tract and the final nucleosomal curvature function, the deformation potential energy E, adopting the first order elasticity model, is given by:

$$E = 1/2b\langle (c(n) - c'(n)) \,|\, (c(n) - c'(n)) \rangle$$

namely a quantity proportional to the square of the modulus of the vectorial difference between the local curvatures, averaged over a 145 bp tract, where

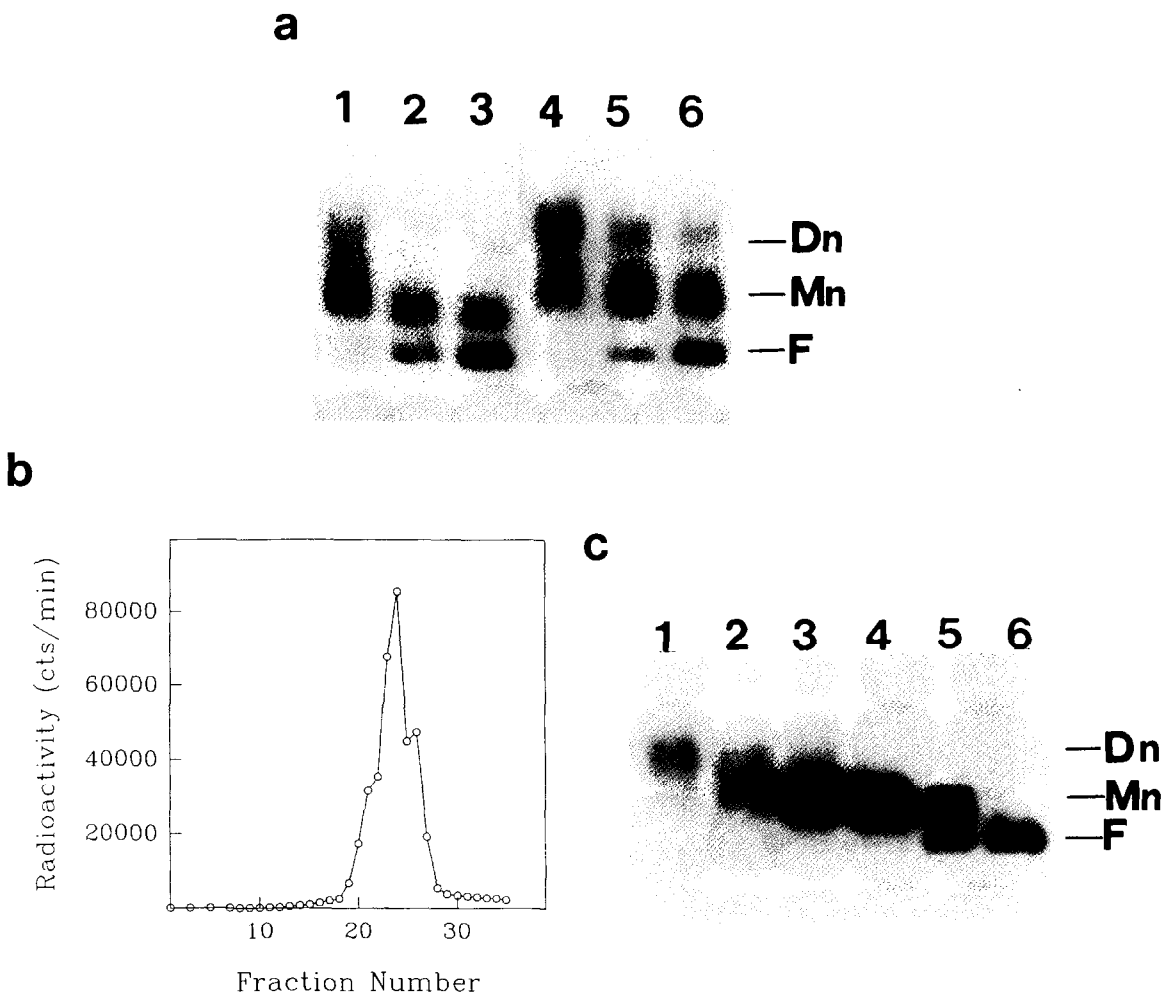

Fig. 3. (a) Mobility of the DNA fragments 384-3A (lanes 1–3) and 384-E9 (lanes 4–6) after reconstitution to form nucleosomes. Nucleosomal DNA added as a competitor: no DNA added, lanes 1, 4; 1 μg, lanes 2, 5; 2 μg, lanes 3, 6. F indicates free DNA, Mn, mononucleosomes, Dn, dinucleosomes. (b) Glycerol gradient analysis of reconstituted mononucleosomes on 5′-labelled 384 bp DNA fragments. (c) Electrophoretic analysis of some of the fractions (from left to right: 18, 20, 23, 24, 27, 29) from the gradient shown in (b).

$$c(n) = \sum_{n\text{th turn}} \mathrm{d}(s)\ \exp(2\pi i s/n)$$

is the curvature at position n of the sequence given in modulus and phase; b, the isotropic elastic bending constant of 145 bp DNA tract; n, the B DNA periodicity and $\mathrm{d}(s) = (\rho\text{-}i\tau)$ the local deviations of the s-th dinucleotide step from the canonical B DNA structure in terms of the roll, ρ, and tilt, τ, angles; and

$$c'(n) = -k \exp[2\pi(n-73)\alpha/145]$$

($k = 43.5°$ except for $60 \leq n \leq 85$ where $k = 0$)

α, the pitch angle of the nucleosomal superhelix $= tg^{-1}28/(2\pi 43)$

Fig. 2 shows the distortion energy profiles obtained for *rbcS-3A* and *rbcS-E9*, by calculating for successive 145 bp tracts along the sequence of the vectorial difference between the local curvature of the DNA tract and the corresponding curvature of the nucleosomal form with both phases referred to the same central 73th bp. The periodical patterns represent the phasing between the intrinsic and induced average curvatures of recurrent 145 bp tracts, and the minima indicate the translational positioning of the virtual nucleosome dyad axis fixed on the pseudo dyad axis of the central

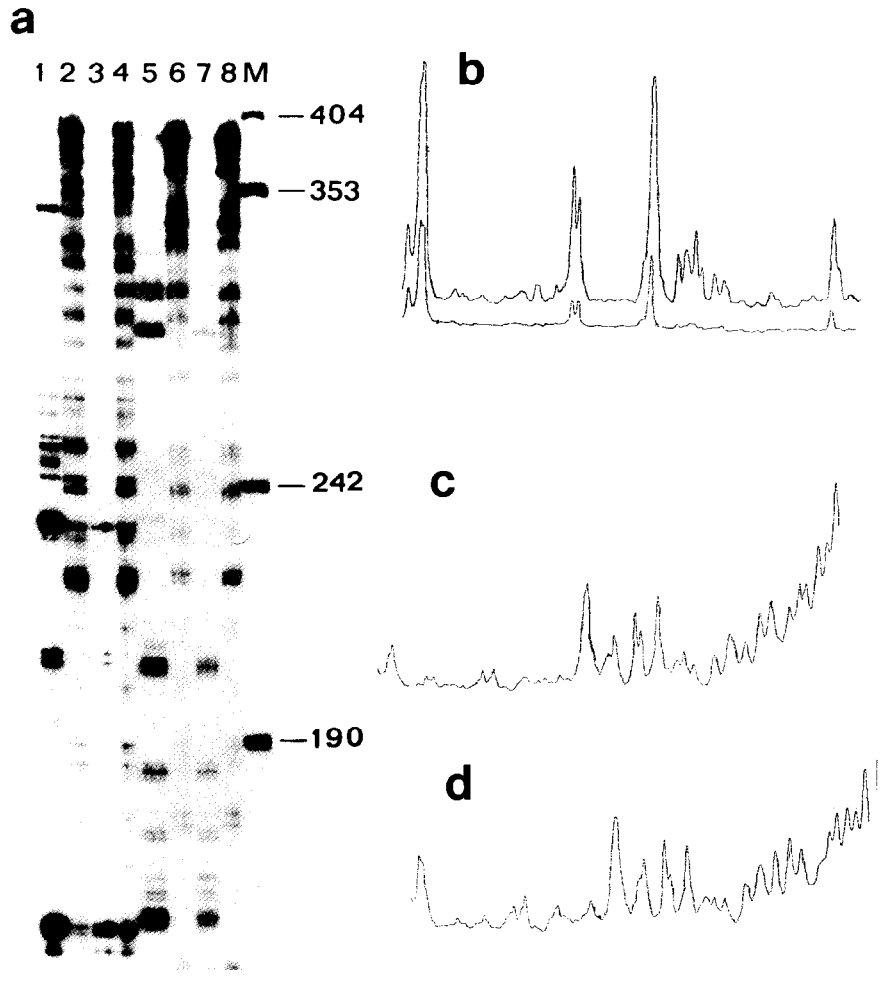

Fig. 4. Exo III digestion of free and reconstituted 384-3A DNA fragment, 5′ labelled at the *Eco*RI site (lanes 1–4) or at the *Bam*HI site (lanes 5–8), analyzed in a 6% denaturing polyacrylamide gel. Free DNA was digested with 40 U of Exo III for 10 min (lanes 1 and 5) and for 30 min (lanes 3 and 7); mononucleosome was digested with 60 U of Exo III for 10 min (lanes 2 and 6) and for 30 min (lanes 4 and 8). M is a pUC19/*Hpa*II digest as a molecular weight standard. In (b) are reported the densitometric profiles of lanes 1 and 3, showing the disappearance after a 30 min digestion of the Exo III stops found after 10 min; (c) and (d) show the densitometric profiles of lanes 2 and 4.

bp. Such a representation is different from that reported in our previous paper [8], where the nucleosome moves along the DNA following the energy minimum pathway which corresponds to the curve fitting the minima of the energy profile in Fig. 2.

In Fig. 2 the deformation energy is reported in kcal/mol of nucleosome adopting a bending constant value of the straight DNA, $b = 2.4 \times 10^{-4}$ kcal/nucleosome degrees^{-2}, deduced from the generally accepted value of the persistence length of a normal DNA equal to 500 Å. The zero energy corresponds to the distortion energy of a straight DNA tract with random or uniform sequence and only the values lower than 3 kcal/nucleosome are reported.

In our case the virtual nucleosome positionings of 384-3A and 384-E9 DNAs appear very different in spite of the remarkably high sequence homology (about 83%, see Fig. 1). In particular, in the case of *rbcS-3A* two main positions are evident at about −200 and −80, and an almost forbidden region around −160, where the required distortion energy is higher than that of straight DNA.

The virtual nucleosome positioning on *rbcS-E9* appears more complex; it is characterized by three main

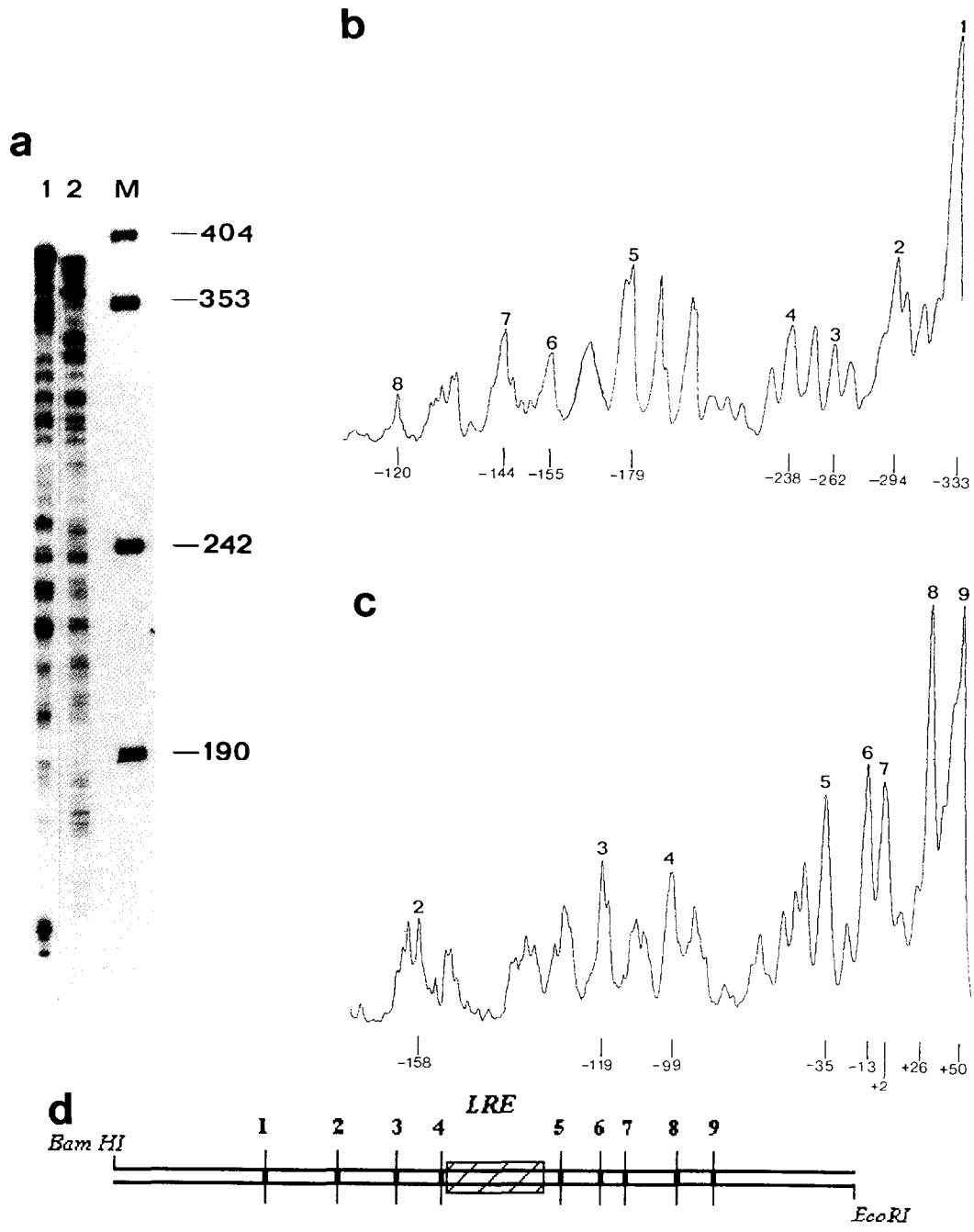

Fig. 5. Reconstituted mononucleosomes on 384-3A, digested with 60 U of ExoIII for 30 min at 30°C. (a) 6% Denaturing polyacrylamide gel. Lane 1, DNA labelled at the *Eco*RI site; lane 2, labelled on the *Bam*HI site. M is a pUC19/*Hpa*II digest. The numbers indicate the centres of distributions of positioned nucleosomes; bands corresponding to the borders of the same nucleosome has the same number. In (b) and (c) the densitometric profiles of lanes 1 and 2 are shown. (d) Localization of the main nucleosome dyad axis positions.

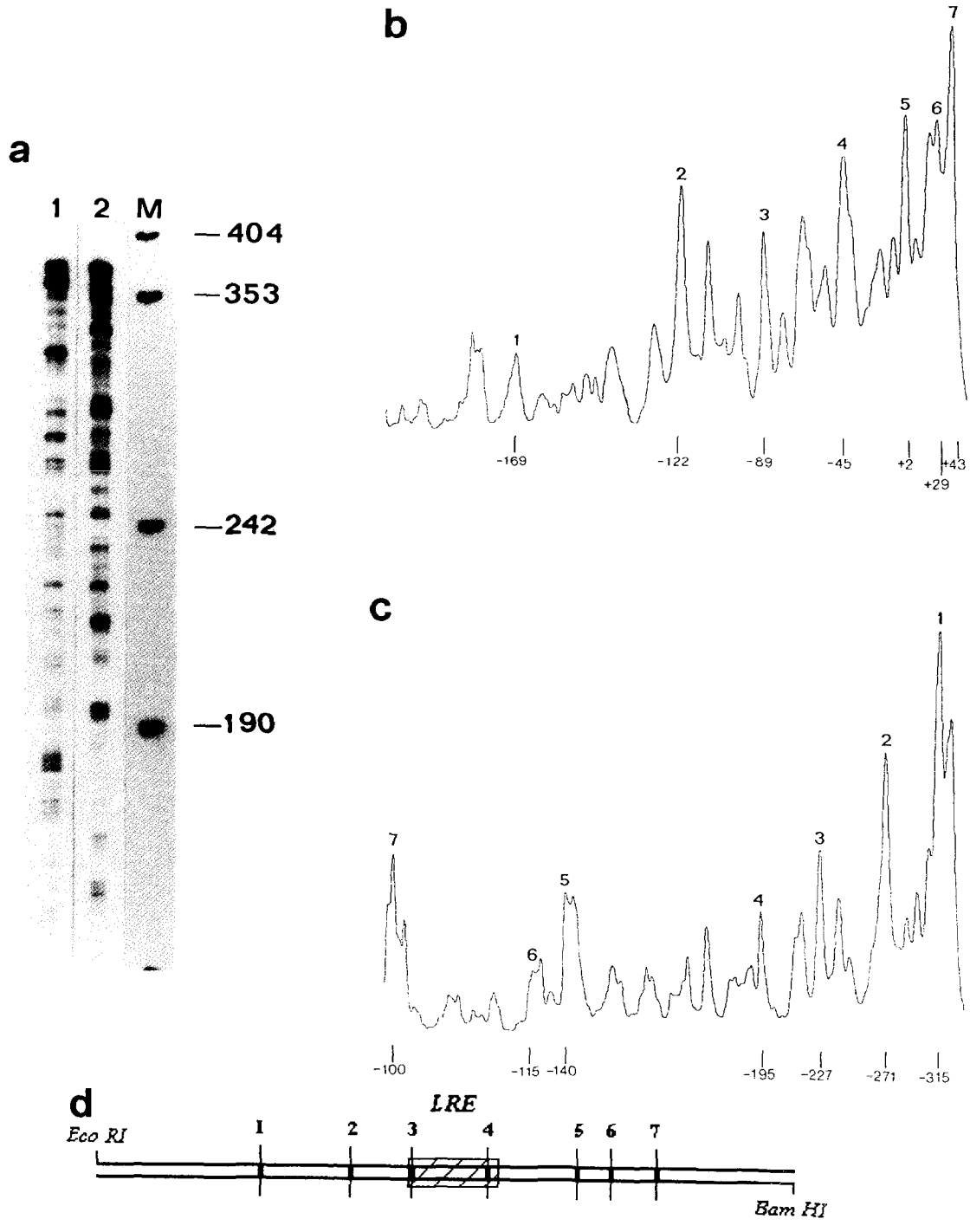

Fig. 6. (a) ExoIII digestion of mononucleosomes reconstituted on 384-E9. Lane 1, DNA labelled at the *Eco*RI site; lane 2, labelled on the *Bam*HI site. M is a pUC19/*Hpa*II digest; (b) and (c), densitometric profiles of lanes 1 and 2, respectively. (d) Localization of the main nucleosome dyad axis positions. For experimental conditions see Fig. 5.

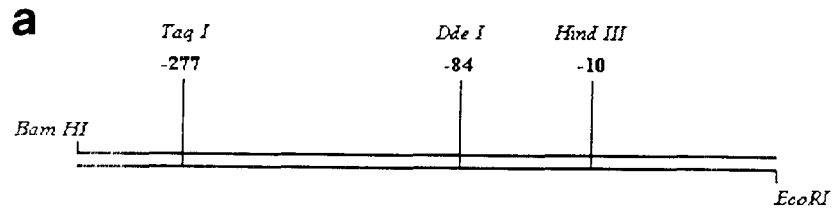

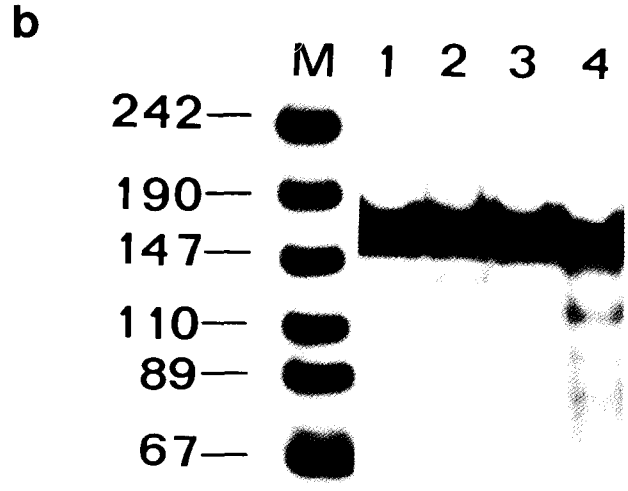

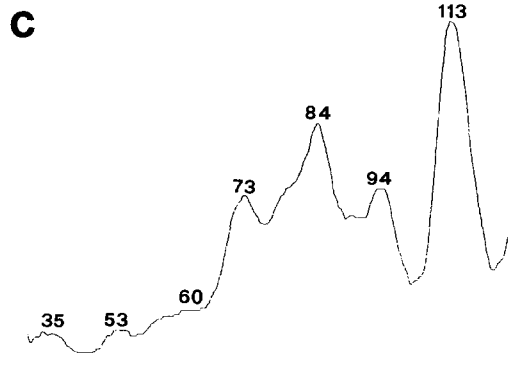

d

enzyme	cleavage site	fragments observed (bp)
Hind III	-10	148, 118, 88/60
Dde I	-84	147, 113/35, 94/53, 84/60,73
Taq I	-277	148, 130, 106, 91/57

Fig. 7. (a) Schematic profile of 384-3A showing sites of the restriction enzymes used in the experiments. (b) Nucleosomal DNA, obtained from micrococcal nuclease digestion of mononucleosomes reconstituted on 384-3A: lane 1, unrestricted; lane 2, cut with *Taq*I; lane 3, cut with *Hin*dIII; lane 4, cut with *Dde*I. (c) Densitometric profile of lane 4. M, pUC19 digested with *Hpa*II. (d) List of the lengths of the DNA fragments after restriction. Samples were run on a 8% native polyacrylamide gel.

positions at about −230, −120, and −40, and two regions with a lower probability of forming nucleosomes, located between −200 and −140, and between −100 and −60. Also in this case, in the region between −210 and −140 the distortion energy is higher than for a straight DNA.

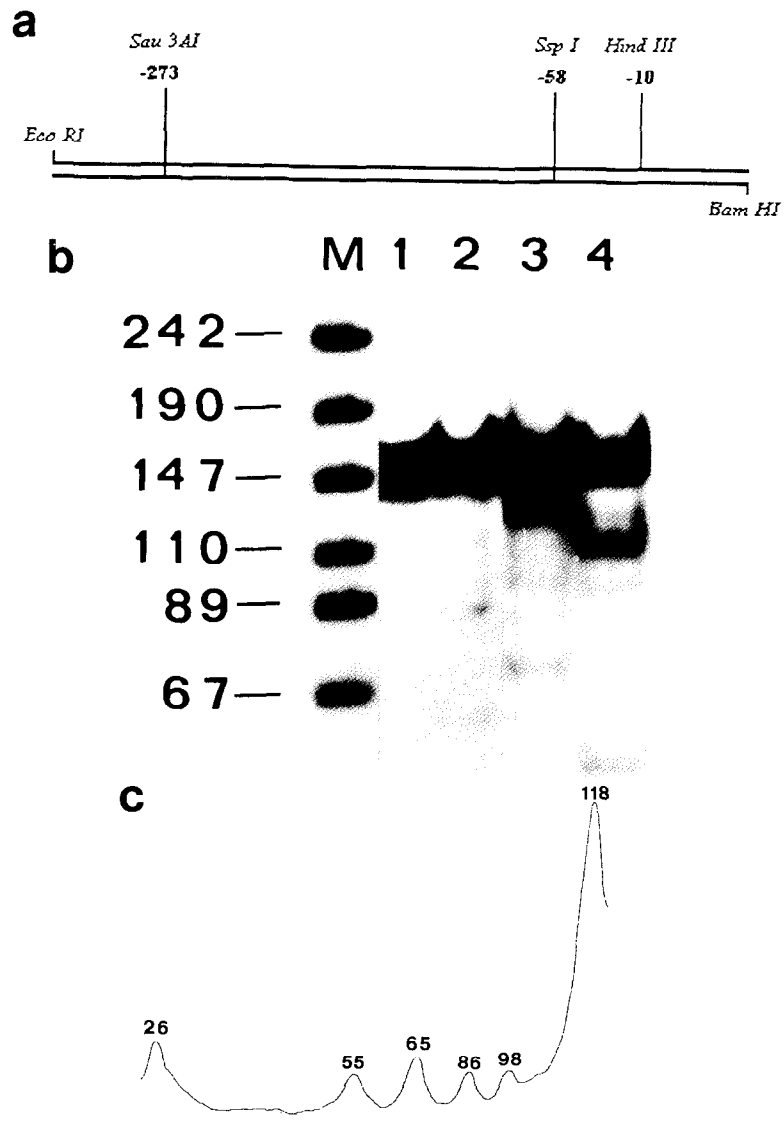

d

enzyme	cleavage site	fragments observed (bp)
Hind III	-10	146, 113, 88
Ssp I	-58	149, 112, 100/52, 84/61
Sau 3AI	-273	147, 118/26, 98/55, 86/65

Fig. 8. (a) Schematic profile of 384-E9 showing sites of the restriction enzymes used in the experiments. (b) Lane 1, unrestricted nucleosomal DNA; lane 2, cut with *Hin*dIII; lane 3, cut with *Sau*3AI; lane 4, cut with *Ssp*I. (c) Densitometric profile of lane 3. (d) List of the lengths of the DNA fragments after restriction. For experimental conditions, see Fig. 7.

It is interesting to note that in all cases the minima of the distortion energy appear as a distribution of very sharp peaks spaced each about 10 bp, predicting a nucleosome multiple translational positioning characterized by the same rotational phasing. The periodicity, evaluated via Fourier transformation, was equal to 10.3

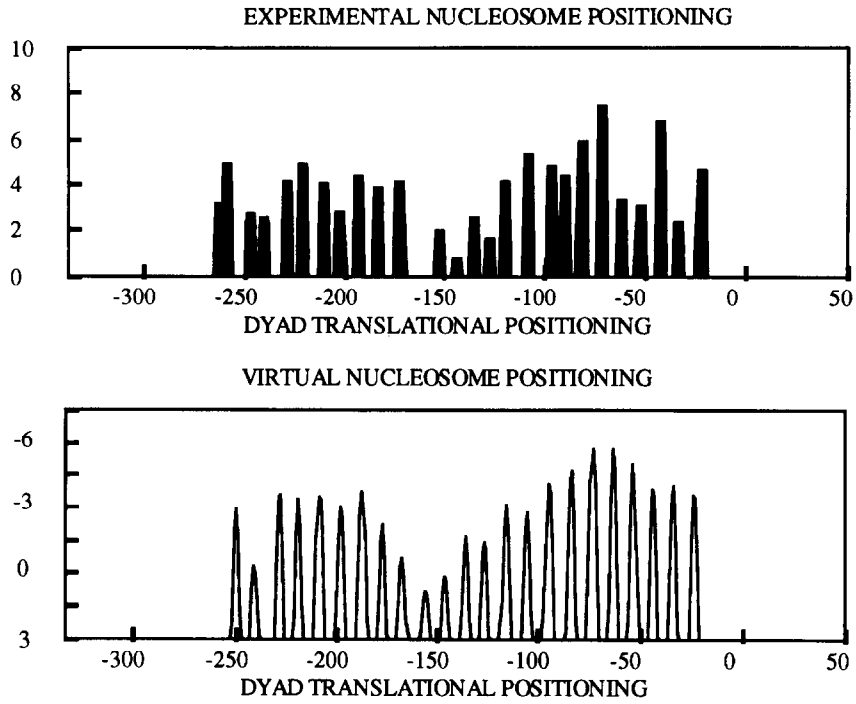

Fig. 9. Comparison between experimental (top) and theoretical (bottom) nucleosome positioning along the 384-3A sequence. On the horizontal axes are indicated the positions of the dyad axis. On the vertical axes, the percentage frequency of the diverse positions from Exo III mapping, and the calculated distortion energies.

in all cases. Such a typical energy pattern is obtained also adopting the Trifonov roll and tilt angles [1], but with some differences in energy values. Finally, a similar pattern is obtained if the occurrence frequency in facing toward the protein core of AA + TT dinucleotide steps in the minor groove is calculated in agreement with the Travers findings [20].

3.2. Monitoring the exchange between nucleosomes and the two 384 bp DNA fragments

The exchange between nucleosomes and the two 384 bp DNA fragments was monitored by agarose gel electrophoresis; the higher molecular weight and reduced charge of the nucleosome with respect to naked DNA causes a reduced electrophoretic mobility.

As shown in Fig. 3a, the reconstituted fragments show two bands of reduced mobility, which can be attributed to dinucleosome and mononucleosome, respectively; in fact, increasing the amount of nucleosomal DNA as competitor, the first decreases and the second increases up to a ratio between fragment and nucleosomal DNA of about 1/10, where only mononucleosome is present. Throughout this research, we have used only this type of reconstitutes.

The presence of only mononucleosomes in our study has been confirmed by the use of density gradients (Fig. 3b). The reconstitution mixture has been applied to 5–30% glycerol gradient and the presence of mononucleosome in different fractions was checked by gel electrophoresis (Fig. 3c). Electrophoretic analysis of the material purified on gradients shows that mononucleosome represents a homogeneous population.

3.3. Nucleosome borders by Exonuclease III analysis

The localization of nucleosome borders was obtained by Exo III digestion. This exonuclease removes nucleotides starting from 3′-ends of double stranded DNA; the presence of a nucleosome blocks the progress of the enzyme. Prominent pauses in the time course of Exo III digestion should, therefore, indicate nucleosome positions [21,22].

Fig. 4 shows Exo III digests of the naked and reconstituted 384-3A DNA fragment 5′-end labelled on either strand, at increasing reaction times; experimental

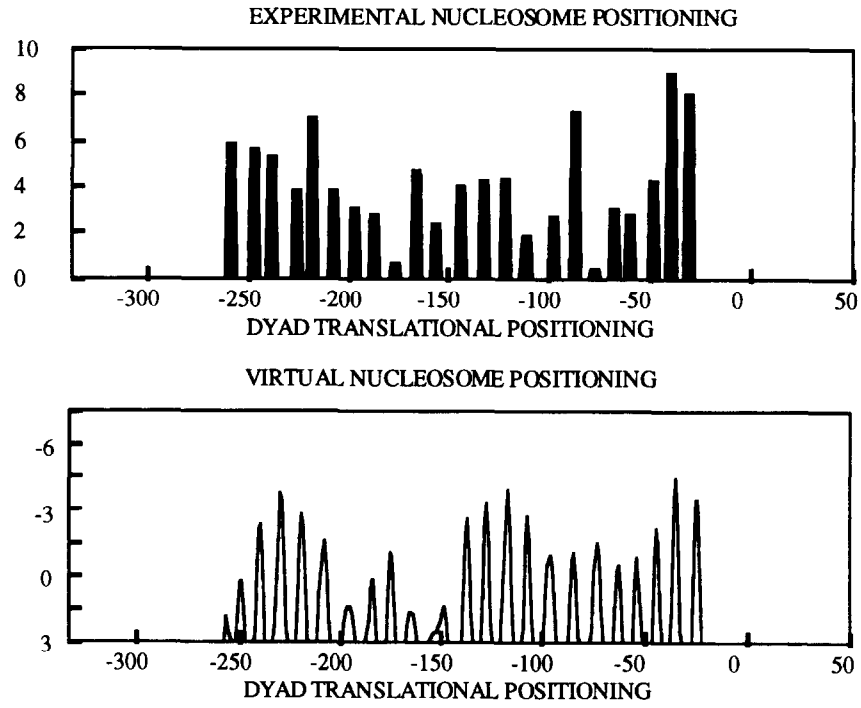

Fig. 10. Comparison between experimental (top) and theoretical (bottom) nucleosome positioning along the 384-E9 sequence. The values on the ordinates are as in Fig. 9.

Table 1
Comparison between nucleosome positioning by Exonuclease III and by restriction enzyme analysis

DNA Fragment	Enzyme	Dyad axis position by RE	Dyad axis positions by Exo III
384-3A	*Hind* III	−25	−23
	Dde I	−44	−47
		−71	−71
		−84	−86
		−105	−108
	Taq I	−220	−221
		−259	−260
384-E9	*Hind* III	−25	−27
		−50	−44
	Ssp I	−31	−30
		−47	−44
		−69	−67
	Sau 3AI	−248	−242

details are reported in the figure legend. The amount of nucleosomal DNA added to the reconstitution mixture assures that in all cases only mononucleosome is present (see Fig. 3a). After 30 min of digestion the band pattern of naked DNA almost disappears, while the positions and intensities of Exo III stops do not change with increasing time, indicating that all mononucleosome main positions have been detected. This finding, together with the observation that the main Exo III stops from mononucleosome digests do not correspond to those from free DNA digests, allow us to assume that all bands from the reconstituted fragment derive from DNA complexed with histone octamer.

The band patterns appear complex, indicating that nucleosomes have more than one preferential location on the sequence considered, and that a number of differently populated sets of molecules with one well positioned nucleosome are present.

To localize nucleosome stops with respect to the DNA sequences, the band patterns have been analyzed as densitometric tracings in both DNA fragments, as reported in Fig. 5 (384-3A) and Fig. 6 (384-E9). Nine main positions, assigned taking into consideration Exo III stops from both directions, are detectable on 384-3A; each one is characterized by the presence of bands of lower intensity differing from the main band of 10–11 bp. The densitometric tracing, deriving from the gel electrophoretic analysis of 384-E9 fragments, reveals

seven main bands; also in this case, the distribution of satellite bands about the main one has a periodicity of 10–11 bp. These results show that nucleosome positioning on the two sequences is characterized by a distribution of preferential locations with the same rotational phasing, but differently populated. The main nucleosome positions emerging from Exo III experiments, indicated as the dyad axis positions, have been reported with respect to the sequence maps in Figs. 5d and 6d. It can be seen that a remarkable difference between the patterns of nucleosome positioning on the two DNA fragments exists; in the case of *rbcS-E9*, two main nucleosome positions are centered in the LRE region, while no nucleosome dyad axes are present in this region in the case of the most expressed gene, *rbcS-3A*.

3.4. Restriction enzymes cleavage analysis of the reconstituted mononucleosomes

In order to obtain further evidence on nucleosome positioning we adopted an independent measurement. Nucleosome monomers were obtained digesting reconstitutes with micrococcal nuclease; the nucleosome-bound DNA was purified and digested with three different restriction enzymes cutting only one time on the two DNA fragments. The rationale of the experiment is that we will obtain undigested DNA if the restriction site is external to the DNA region occupied by a nucleosome, and two fragments if the restriction site is inside a positioned nucleosome. However, if multiple positions are present, a number of fragments would be obtained by each restriction enzyme digest [23,24]. The central region of the fragment cannot be analyzed with this method because of the lack of unique restriction sites and the difficulty to assign an univocal nucleosomal position from digested fragments. A large amount of undigested DNA is predicted, since several different positions for the mononucleosome have been found by nucleosome theoretical prediction and by Exo III specific cleavage. In fact, for both fragments we found a remarkable amount of undigested DNA (see Figs. 7 and 8). At the moment, the restriction enzyme analysis must be considered mainly qualitative and from the size of the restriction fragments it is possible to estimate the nucleosome positions, as reported in Figs. 7d and 8d.

From the results obtained, a nucleosome multiple positioning with the same rotational phasing clearly appears. Therefore, this feature of nucleosome positioning is confirmed by an independent approach with respect to Exo III analysis, ruling out, as previously shown [23–25], effects due to enzyme invasion of nucleosomes [22].

4. Discussion

The correlation between theoretical nucleosome positioning and experimental mapping from Exo III digestion can be evaluated by deriving, from gel electrophoresis densitometric tracings, the preferential locations of nucleosome dyad axis along the sequence.

To this end, we have considered densitometric tracings from a number of different experiments, each consisting of two densitometric profiles derived from the Exo III digestion of the same fragment labeled on the two 5′-ends. With this approach it is possible to derive the dyad location from two independent measurements of the same experiment. Furthermore, considering a number of densitometric profiles from different experiments, we have averaged the nucleosome location frequency.

The results are shown in Figs. 9 and 10, and for many positions of the dyad axis result in fairly good agreement with those obtained with restriction enzyme mapping and reported in Table 1. Figs. 9 and 10 also show the comparison between experimental mapping and theoretical distortion energy profiles. The theoretical profiles are the same as shown in Fig. 2, but with the scale inverted in the ordinate direction for sake of comparison. The agreement between theoretical and experimental nucleosome positioning is very satisfactory, if we consider the probability of the different DNA regions to be organized in a mononucleosome. If we consider the two positionings in detail, namely the frequency of nucleosome population for the different positions of the dyad axis, some differences are evident, mainly in the case of *rbcS-E9*.

From the reported results, some general considerations can be derived.

4.1. Relevance of DNA intrinsic curvature, as predicted by the nearest-neighbor approximation, in nucleosome positioning

The good agreement between the theoretical prediction and experimental mapping of nucleosomes in the two sequences examined demonstrates that DNA intrinsic curvature has a dominant role in nucleosome positioning, and is in agreement with previous results from many synthetic and biological systems [19,25,26].

Furthermore, since our theoretical prediction derives from the nearest-neighbor approximation [7,8], the results obtained show that this simple model is reliable (using the same matrix of roll and tilt angles) in predicting DNA physico-chemical properties, such as gel electrophoretic mobilities [4,5], cyclization probabilities [6], as well as specific interactions with histone octamer ([7,8], this paper).

However, it is worth noting that the comparison between nucleosome theoretical and experimental mapping (see Figs. 9 and 10) shows that the population of some nucleosome minima is remarkably different. This could derive from inherent features of nucleosome cleavage by Exo III as previously discussed by Shrader and Crothers [26], as well as by local specific interactions between histone side chains and DNA bases; this topic, however, deserves further investigation.

4.2. Nucleosome multiple positioning from theoretical and experimental mapping

Nucleosome multiple positioning with the same rotational phasing was found both by Exo III and restriction enzyme mapping, for the two sequences examined, and appears as a common feature of all the positions of the dyad axis. Nucleosome multiple positioning can be considered as characteristic of many investigated systems in vitro and in vivo [11,25] and was clearly shown by van Holde and co-workers [24] to correspond to equilibrium distributions, that arise from differences in energy of about 1 kcal/nucleosome.

Considering the nucleosome theoretical distributions of the dyad axis, it is interesting to note that whilst energy differences in nucleosome rotational positioning are of the order of 10 *RT* about the minima of the energy diagrams, changes in the translational positioning nearby the energy minima require an energy cost of the order of *RT*. This explains the finding that phasing of nucleosomes is sequence dependent whereas the translational positioning, about a minimum, appears to be less predictable.

Finally, it is tempting to comment on the possible relevance of our study with respect to the different transcription efficiency of the two genes, considering the high sequence homology of the two upstream regulative sequences (see Fig. 1). The absence of nucleosomes centered on the LRE of the most expressed gene, *rbcS-3A*, suggests that a different accessibility of these sequences to regulatory proteins could contribute to explain the difference in the expression of the two genes.

Acknowledgements

We wish to thank Dr. Nam-Hai Chua and Dr. Chris Kuhlemeier for the clones pUC18-3A/E9 and pBR325-E9. The financial support of the Fondazione Istituto Pasteur-Fondazione Cenci Bolognetti is gratefully acknowledged. Thanks are due to Roberto Gargamelli for his technical aid.

References

[1] A. Bolshoij, P. McNamara, R.E. Harrington and E.N. Trifonov, Proc. Natl. Acad. Sci. USA 88 (1991) 2312.
[2] P. De Santis, S. Morosetti, A. Palleschi and M. Savino, in: Structures and dynamics of nucleic acids, proteins and membranes, eds E. Clementi and S. Chin (Plenum, New York, 1986) p. 31.
[3] P. De Santis, A. Palleschi, M. Savino and A. Scipioni, Biophys. Chem. 32 (1988) 305.
[4] S. Cacchione, P. De Santis, D. Foti, A. Palleschi and M. Savino, Biochemistry 28 (1989) 8706.
[5] P. De Santis, A. Palleschi, M. Savino and A. Scipioni, Biochemistry 29 (1990) 9269.
[6] S. Cacchione, P. De Santis and M. Savino, FEBS Letters 336 (1993) 293.
[7] D. Boffelli, P. De Santis, A. Palleschi and M. Savino, Biophys. Chem. 39 (1991) 127.
[8] P. De Santis, M. Fuà, A. Palleschi and M. Savino, Biophys. Chem. 46 (1993) 193.
[9] D. Rhodes, EMBO J. 4 (1985) 3473.
[10] G. Felsenfeld, Nature 355 (1992) 219.
[11] A.P. Wolffe, Cell 77 (1994) 13.
[12] R. Fluhr, P. Moses, G. Morelli, G. Coruzzi and N.-H. Chua, EMBO J. 5 (1986) 2063.

[13] C. Kuhlemeier, R. Fluhr and N.-H. Chua, Mol. Gen. Genet. 212 (1988) 405.
[14] C. Kuhlemeier, P.J. Green and N.-H. Chua, Annu. Rev. Plant Physiol. 38 (1987) 221.
[15] P.J. Green, S.A. Kay and N.-H. Chua, EMBO J. 6 (1987) 2543.
[16] G. Coruzzi, R. Broglie, C. Edwards and N.-H. Chua, EMBO J. 3 (1984) 1671.
[17] P. Forte, L. Leoni, B. Sampaolese and M. Savino, Nucleic Acids Res. 17 (1989) 8683.
[18] H.R. Drew and A.A. Travers, J. Mol. Biol. 186 (1985) 773.
[19] A.A. Travers and A. Klug, Phil. Trans. Roy. Soc. 317 (1987) 537.
[20] A.A. Travers, Ann. Rev. Biochem. 58 (1989) 427.
[21] N. Ramsay, J. Mol. Biol. 189 (1986) 179.
[22] A. Prunell, Biochemistry 22 (1984) 4887.
[23] J.C. Hansen, J. Ausio, V.H. Stanik and K.E. van Holde, Biochemistry 28 (1989) 9129.
[24] F. Dong, J.C. Hansen and K.E. van Holde, Proc. Natl. Acad. Sci. USA 87 (1990) 5724.
[25] M. Buttinelli, E. Di Mauro and R. Negri, Proc. Natl. Acad. Sci. USA 90 (1993) 9315.
[26] T.E. Shrader and D.M. Crothers, J. Mol. Biol. 216 (1990) 69.
[27] Devereux, Haeberli and Smithies, Nucleic Acids Res. 12 (1984) 387.